The calculation and evaluation for n+^{54,56,57,58}Fe reactions

Yinlu Han[1,a], Yongli Xu[2], Hairui Guo[3], Zhengjun Zhang[4], Haiying Liang[1], Chonghai Cai[5], and Qingbiao Shen[1]

[1] Key Laboratory of Nuclear Data, China Institute of Atomic Energy, PO Box 275(41), Beijing 102413, P.R. China
[2] School of Physics and Electronic Science, Shanxi Datong University, Datong 037009, P.R. China
[3] Institute of Applied Physics and Computational Mathematics, Beijing 100094, P.R. China
[4] Department of Physics, Northwest University, Xi'an 710069, P.R. China
[5] Department of Physics, Nankai University, Tianjin 300071, P.R. China

Abstract. All cross sections of neutron-induced reactions, angular distributions, double differential cross sections, angle-integrated spectra, γ-ray production cross sections and energy spectra for ^{54,56,57,58}Fe are calculated by using theoretical models at incident neutron energies from 0.1 to 200 MeV. The present consistent theoretical calculated results are in good agreement with recent experimental data. The present evaluated data are compared with the existing experimental data and evaluated results from ENDF/B-VII, JENDL-4, JEFF-3, and the results are given in ENDF/B format.

1. Introduction

The deep understanding of nucleon-induced reactions is a crucial step for the further development of nuclear reactions theory in general. In addition, complete information in this field is strongly needed for a large amount of applications, such as the Accelerator-Driven clean nuclear power System (ADS) has been an interesting focus in nuclear physics. They require accurately nuclear reaction data of common cross sections and especially need the data of neutron and proton induced energy-angle correlated spectra of secondary light particles as well as double differential cross sections, γ-ray production cross sections and γ-ray production energy spectra. The development of high-quality nuclear data for iron is particularly important due to their role as an important structural and target material in many accelerator-driven system designs.

In this work, all cross section, angular distribution, the angle-integrated spectra and double differential cross sections of neutrons, protons, deuteron, triton, helium and alpha-particle emissions for n+^{54,56,57,58,nat}Fe reactions are consistent calculated using nuclear theoretical models over the incident neutron energy up to 200 MeV. The integrate the optical model, the intra-nuclear cascade model, the distorted wave Born approximation theory, preequilibrium and equilibrium reaction theories are used. The calculated results are compared with new experimental measured data and the evaluated results.

Section 2 provide a description of the theoretical models and parameters used in this work. Section 3 give analysis and comparisons of the calculated results with the experimental data. Sect. 4 give simple conclusion.

2. Theoretical models and parameters

The optical model is used to describe measured neutron-induced total, nonelastic, elastic cross section and elastic scattering angular distributions, and the measured charged particles-induced total reaction cross sections and elastic scattering angular distributions, and to calculate the transmission coefficient of the compound nucleus and the pre-equilibrium emission process for all particles (neutron, proton, deuteron, triton, helium and alpha-particle). The optical model potentials considered here are Woods-Saxon [1] type for the real part, Woods-Saxon and derivative Woods-Saxon type for the imaginary parts corresponding to the volume and surface absorptions and the Thomas form for the spin-orbit part, respectively. The theoretical model code APMN [2] is used to obtain optical model potential parameters. By this code the best neutron optical model potential parameters at incident neutron energy up to 250 MeV are obtained automatically to fit the experimental data of total, nonelastic, elastic cross sections and elastic scattering angular distributions for n+^{56}Fe reaction.

The local proton optical potential parameters [3] for p+^{56}Fe reaction are obtained from the experimental data of total reaction cross section and elastic scattering angular distributions at incident proton energy up to 250 MeV. The optical potential parameters for deuteron, triton, helium and alpha-particle are taken from the global optical potential parameters [4–7] with incident energies from threshold up to 200 MeV, based on the experimental data of particle total reaction cross sections and elastic scattering angular distributions, respectively.

The unified Hauser-Feshbach and exciton model [8] are used to describe the nuclear reaction equilibrium and preequilibrium decay processes at incident neutron energies below 20 MeV. The Hauser-Feshbach model with width fluctuation correction describes the particle

[a] e-mail: hanyl@ciae.ac.cn

emissions from compound nucleus to the discrete levels and continuum states of the residual nuclei in equilibrium processes, while the preequilibrium process is described by the angular momentum and parity dependent exciton model. The emissions to the discrete level and continuum states in the multi-particle emissions for all opened channels are included. The secondary particle emissions are described by the multi-step Hauser-Feshbach model at incident neutron energies below 20 MeV. The recoil effects in multi-particle emissions from continuum state to discrete level as well as from continuum to continuum state are taken into account strictly, so the energy balance is held accurately in every reaction channels. The double differential cross sections of neutron and proton emissions are calculated with the linear momentum dependent exciton state density model [9]. The double differential cross sections of deuteron, triton, helium and alpha-particle emissions are calculated with the improved Iwamoto-Harada model [10–13].

The preequilibrium statistical theory based on the exciton model, the evaporation models and the Hauser-Feshbach theory with width fluctuation correction, and the intranuclear cascade model are used to describe the nuclear reaction preequilibrium and equilibrium decay processes for incident neutron energies above 20 MeV. The improved Iwamoto-Harada model is used to describe the composite particle (d, t, ^{3}He, α) emission in compound nucleus. The improved Iwamoto-Harada model is included in the exciton model for the light composite particle emissions.

The preequilibrium mechanism of γ-ray emission is also taken into account. The level density parameters and pair correction parameters of the Gilbert-Cameron level density [14] for low energy are used. The Ignatyuk model [15] is particularly appropriate for the relatively high energies and used. The direct reaction are calculated by the distorted wave Born approximation theory. The code DWUCK4 [16] of the distorted wave Born approximation theory is used to pre-calculate the direct inelastic scattering cross sections and angular distributions of discrete levels. The experimental data of inelastic scattering angular distributions for discrete levels are used to guide theoretical calculations. The deformation parameters for excited levels are obtained.

The UNF [17] code is used at incident neutron energies below 20 MeV. The MEND code is used up to 200 MeV. The angular momentum and parity dependent exciton model is used in UNF code, other models are the same as MEND [18] code. The parameters of the level densities and pair correction are taken from RIPL [19], and adjusted by fitting the experimental data of some channel reaction cross sections.

3. The results and analysis

All cross sections, the angle-integrated spectra and angular distributions for n+^{54,56,57,58,nat}. Fe reactions are calculated and compared with the experimental data and the evaluated results from ENDF/B-VII, JENDL-4 and JEFF-3. The comparison of the total and nonelastic cross sections with experimental data for n+^{56}Fe reaction are given in Fig. 1 and Fig. 2. The evaluated data from ENDF/B-VII are lower than those of our present results and experimental data [20] for incident neutron energy from 50.0 to 100.0 MeV. The

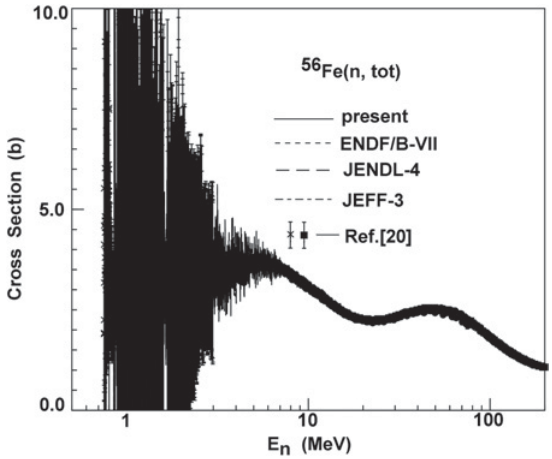

Figure 1. Calculated total cross sections of n+^{56}Fe reaction compared with the experimental data [20].

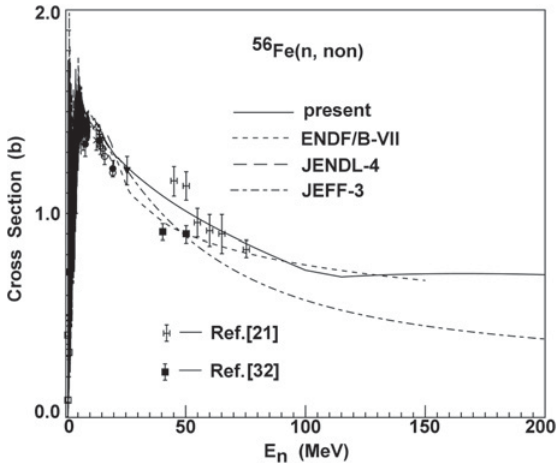

Figure 2. Calculated nonelastic cross sections of n+^{56}Fe reaction compared with the experimental data.

present results are in agreement with the results from JEFF-3. The calculated results of nonelastic cross sections are in very good agreement with new experimental data [21] for incident neutron energy above 20.0 MeV. The evaluated data of a nonelastic cross section from ENDF/B-VII and JEFF-3 are lower than those of our present results for some incident neutron energies.

The calculated results of elastic and inelastic scattering angular distributions for n+^{54,56}Fe reactions are compared with experimental data below at incident energy below 75.0 MeV. The present calculated results are in good agreement with new experimental data.

Since the measured data [22] of inelastic cross sections for n+^{56}Fe reaction demonstrate a lot of fluctuations structure below 4.0 MeV, the calculated results reasonable pass through the experimental data. The present evaluated results adopt the experimental data for different excited states below 4.0 MeV. Figure 3 is the comparisons of present results of inelastic scattering cross sections of the first excited state with experimental data [22,23]. There are some experimental data of total inelastic scattering cross sections. The present results pass through experimental data. The comparisons of present results of total inelastic scattering cross sections with experimental data [22] for ^{56}Fe are given in Fig. 4.

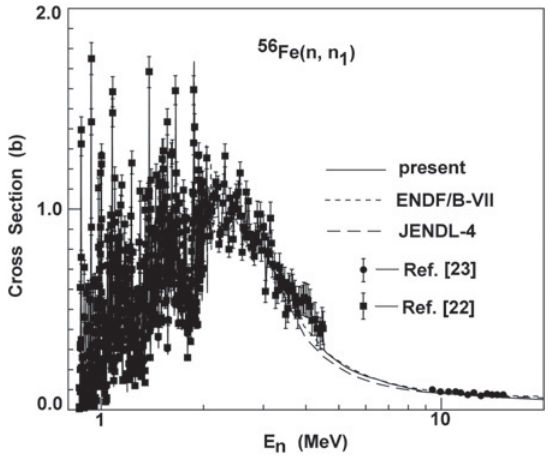

Figure 3. Calculated inelastic cross sections of the first excited state for ^{56}Fe compared with experimental data [22,23].

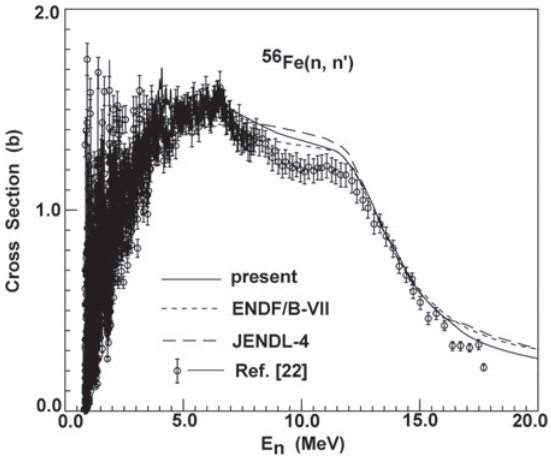

Figure 4. Calculated inelastic cross sections of n+^{56}Fe reaction compared with the experimental data [22].

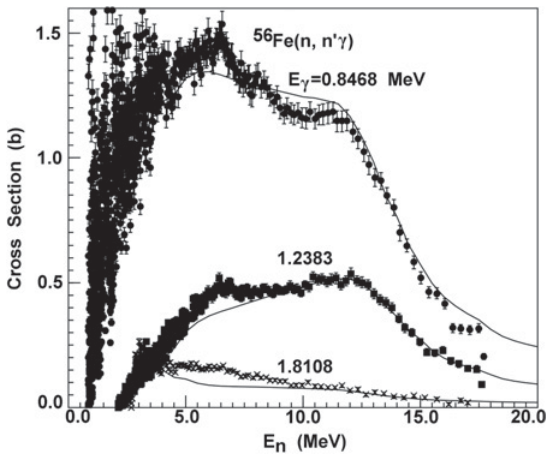

Figure 5. Calculated (n, n′γ) cross sections of n+^{56}Fe reaction compared with the experimental data [22].

The gamma productions cross section for the transitions of the excited state to the ground state and different excited states of n+^{56}Fe reaction were measured in different laboratories. The calculated results of (n, n′γ), (n, pγ), (n, $\alpha\gamma$) and (n, 2nγ) reactions are in agreement with the experimental data [22,24]. The comparisons of calculated results with experimental data for some excited states are only given in Figs. 5 to 8.

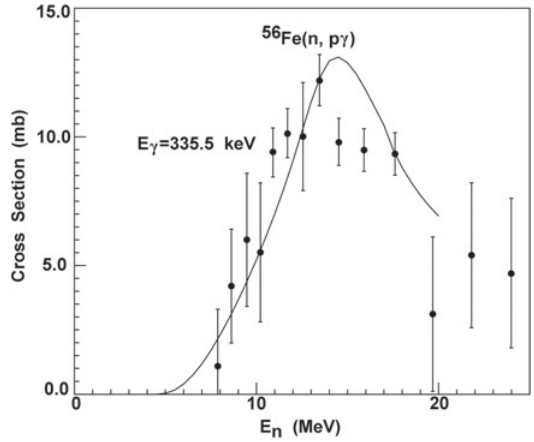

Figure 6. Calculated (n, pγ) cross sections of n+^{56}Fe reaction compared with the experimental data [24].

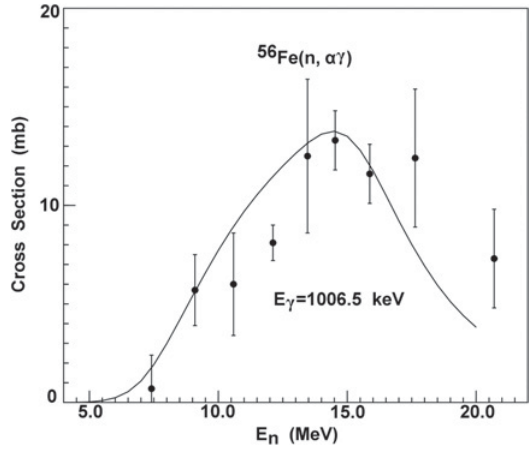

Figure 7. Calculated (n, $\alpha\gamma$) cross sections of n+^{56}Fe reaction compared with the experimental data [24].

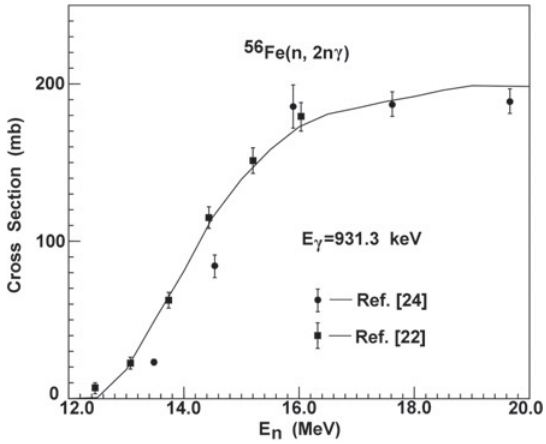

Figure 8. Calculated (n, 2nγ) cross sections of n+^{56}Fe reaction compared with the experimental data [22,24].

We assume we are not too far off from the correct answer for those reaction cross sections, since our prediction partially contributes to the gamma production cross section of the excited state to the ground state and different excited states.

The present results of reaction cross section for all channels are similar to the evaluated results in ENDF/B-VII, JENDL-4 and JEFF-3 in curve shapes, but much better fit experimental data for some channels.

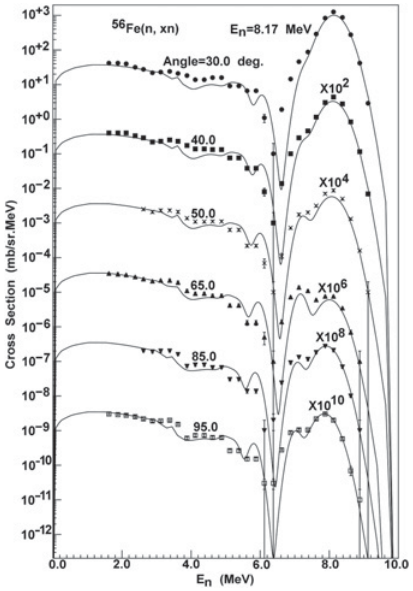

Figure 9. Calculated double differential cross sections of neutron emission compared with the experimental data [25].

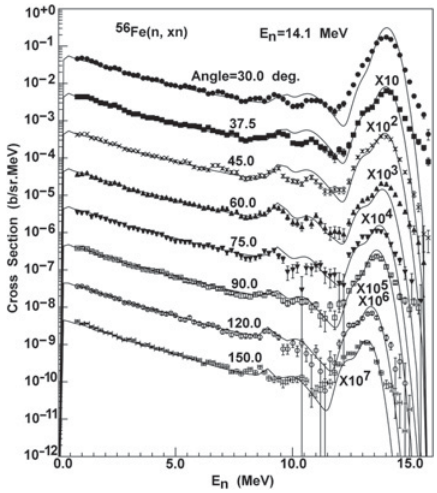

Figure 10. Calculated double differential cross sections of neutron emission compared with the experimental data [26].

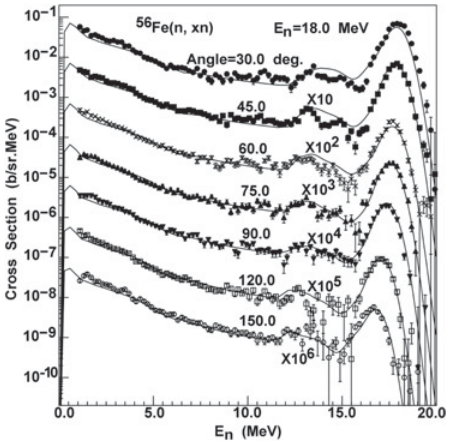

Figure 11. Calculated double differential cross sections of neutron emission compared with the experimental data [27].

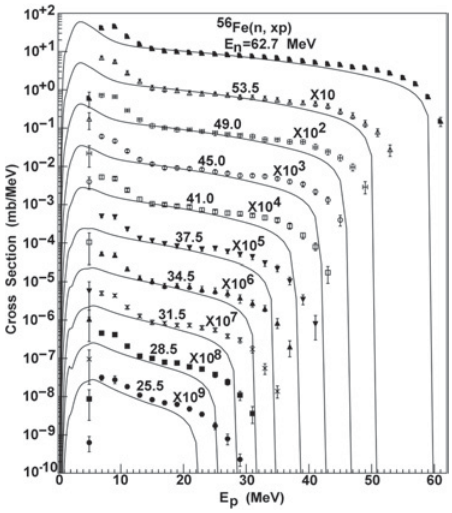

Figure 12. Calculated energy spectra of proton emission compared with the experimental data [29].

Based on the agreements of calculated results with experimental data for all reaction cross section and angular distributions, the energy spectrum and double differential cross section for neutron, proton, deuteron, triton, helium and alpha emission, γ-ray production cross sections and γ-ray production energy spectrum for n+$^{54,56,57,58,\,nat.}$ Fe reactions are calculated by theoretical models.

The calculated results of double differential cross sections of neutron emission for n+^{56}Fe at incident neutron energies below 150.0 MeV are compared with the experimental data. The calculated results are in good agreement with experimental data over the whole emission neutron angles at incident neutron energies below 65.0 MeV. The comparisons between the calculated results and experimental data [25–27] at incident neutron energies 8.17, 14.1 and 18.0 MeV are given in Figs. 9 to 11. The calculated results are in basic agreement with experimental data [28] over the whole emission neutron angles at incident neutron energy below 150.0 MeV.

The calculated results for proton emission energy spectra at incident neutron energy 25.5, 28.5, 31.5, 34.5, 37.5, 41.0, 45.0, 49.0, 53.5 and 62.7 MeV for n+^{56}Fe reaction are compared with experimental data [29] as shown in Fig. 12. The shape and magnitude of the curve representing the calculated results at all incident neutron energy are in good agreement with those of experimental data. The calculated results are lower than those of the experimental data for higher energy proton emission.

The calculated results for alpha emission energy spectra are compared with experimental data [29] at incident neutron energy 41.0, 45.0, 49.0, 53.5 and 62.7 MeV as shown in Fig. 13. The shape and magnitude of calculated results curve for alpha emission are in good agreement with those of experimental data in all alpha particles emission energy. The general trend observed is a decreasing emission probability with increasing emission alpha energy. A quasi-isotropic component is observed at very low energy (0–15 MeV), where are mainly from the contributions of equilibrium reaction.

The calculated results of the energy spectra of particle emission at incident neutron energy 96.0 MeV for n +^{56}Fe

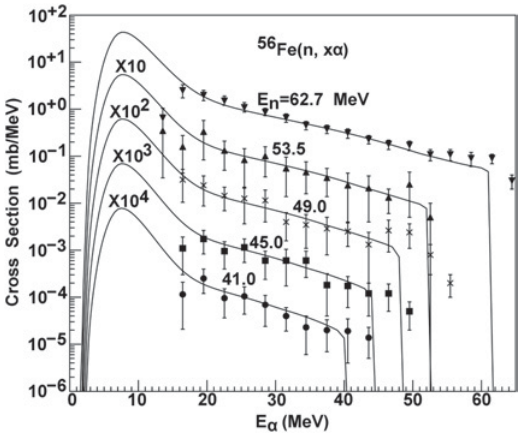

Figure 13. Calculated energy spectra of alpha emission compared with the experimental data [29].

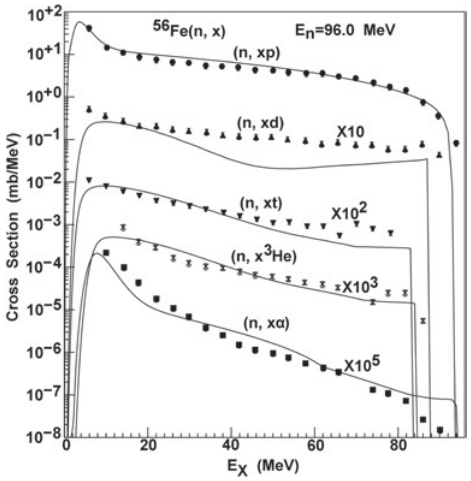

Figure 14. Calculated energy spectra of proton, deuteron, triton, ^{3}He and α emission compared with the experimental data [30].

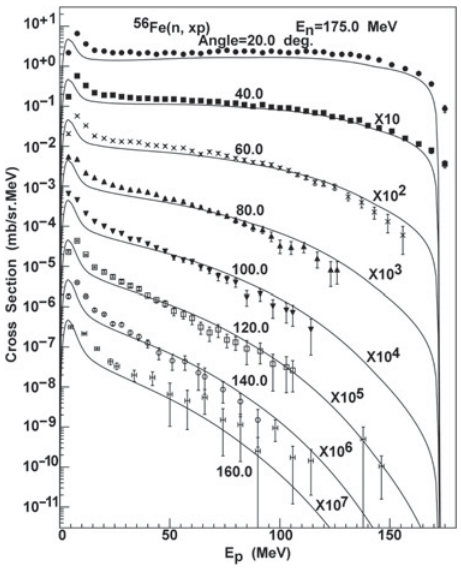

Figure 15. Calculated double differential cross sections of proton emission compared with the experimental data [31].

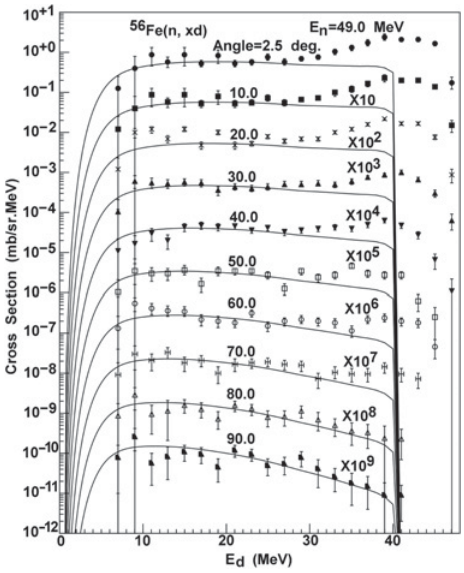

Figure 16. Calculated double differential cross sections of deuteron emission compared with the experimental data [29].

reaction are compared with experimental data [30] in Fig. 14. The shape and magnitude of calculated results curve for proton, triton, helium and alpha emission are in good agreement with those of experimental data in all particle emission energy regions. The calculated results are in agreement with experimental data for low energy deuteron emission region, and lower than experimental data for higher energy deuteron emission region, where are from the contribution of direct reaction. Since the improved Iwamoto-Harada model is only included in pre-equilibrium emission processes in present work, if the knocking-out reaction is included, the calculated results may be improved for high energies deuteron emission.

The calculated results of the double differential cross sections of proton emission at incident neutron energy 175.0 MeV for n $+^{56}$Fe reaction are compared with experimental data [31] in Fig. 15. The shape of calculated results curve for proton emission energy spectra is in good agreement with those of experimental data.

The double differential cross sections of emission deuteron are compared with experimental data [29] at incident neutron energy 49.0 MeV. The magnitude and shape of calculated results curve are consistent with the experimental data in Fig. 16.

The double differential cross sections of triton emission are compared with experimental data [31] as shown in Fig. 17. The magnitude and shape of calculated results curve are in good agreement with experimental data. The double differential cross sections of helium emission are compared with experimental data [31] as shown in Fig. 18. The magnitude and shape of calculated results curve are in good agreement with experimental data. Figures 17 and 18 also show the double differential cross sections of emission triton and helium are similar at incident neutron energy 175.0 MeV. The energy spectra and double differential cross section of neutron, proton, deuteron, triton, helium and alpha emission for n $+^{54,57,58}$Fe reactions are also calculated and analyzed. The results are similar to those of n$+^{56}$Fe reaction.

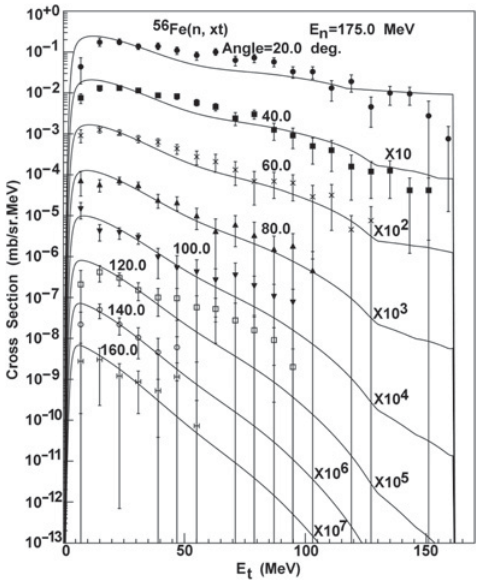

Figure 17. Calculated double differential cross sections of triton emission compared with the experimental data [31].

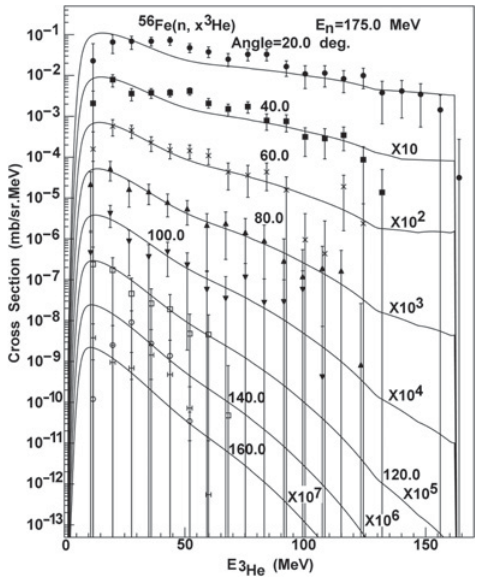

Figure 18. Calculated double differential cross sections of ^{3}He emission compared with the experimental data [31].

4. Conclusions

Based on the optimal neutron optical potential parameter, all cross sections of neutron induced reactions and angular distributions, the energy spectra and double differential cross sections for ^{54,56,57,58}Fe are consistent calculated using nuclear theory models at incident neutron energies from 0.1 to 200 MeV. Since the recoil effect is taken into account, the energy for whole reaction processes is balance. Good agreement is generally observed between the calculated, evaluated results and the experimental data. Since the improved Iwamoto-Harada model is included in the exciton model for the light composite particle emissions, the theoretical models provide the good description of the shapes and magnitude of the energy spectra and double differential cross section of deuteron, triton, helium and alpha emission. The present results have been transformed into ENDF/B formatted data files for application.

In order to improve the energy spectra and double differential cross sections of deuteron emission above incident neutron energy 65.0 MeV, the theoretical model must include the knock-out mechanism.

This work is supported by China National Natural Science Foundation-NSAF under Grant No. U1630122. This work was part of National Basic Research Program of China (973 Program), and was supported by the China Ministry of Science and Technology under Contract No. 2007CB209903.

References

[1] JR. F.D. Becchetti, G.W. Greenlees, Phys. Rev. **182**, 1190 (1969)
[2] Qingbiao Shen, Nucl. Sci. Eng. **141**, 78 (2002)
[3] Yinlu Han, Yue Zhang, Hairui Guo, Nucl. Instr. Meth. B **265**, 461 (2007)
[4] Yinlu Han, et al., Phys. Rev. C **74**, 044615 (2006)
[5] Yongli Xu, Hairui Guo, Yinlu Han, Qingbiao Shen, Sci. China Phys. Mech. Astron. **54**, 2005 (2011)
[6] Yong-Li Xu, Hai-Rui Guo, Yin-Lu Han, Qing-Biao Shen, Int. J. Mod. Phys. E **24**, 1550005 (2015)
[7] Xin-Wu Su, Yin-Lu Han, Int. J. Mod. Phys. E **24**, 1550092 (2015)
[8] Jingshang Zhang, Nucl. Sci. Eng. **114**, 55 (1993)
[9] M.B. Chadwick and P. Oblozinsky, Phys. Rev. C **44**, R1740 (1991)
[10] A. Iwamoto, K. Harada, Phys. Rev. C **26**, 1821 (1982)
[11] J.S. Zhang, et al., Z. Phys. A **344**, 251 (1992)
[12] J.S. Zhang, Nucl. Sci. Eng. **116**, 35 (1994)
[13] Qingbiao Shen, Nucl. Sci. Eng. **117**, 99 (1994)
[14] W. Dilg, et al., Nucl. Phys. A **217**, 269 (1973)
[15] A.V. Ignatyuk, et al., Sov. J. Nucl. Phys. **21**, 255 (1975)
[16] P.D. Kunz, Distorted Wave Code DWUCK4. University of Colorado (1994)
[17] Jingshang Zhang, Nucl. Sci. Eng. **142**, 207 (2002)
[18] Chong-hai Cai, Nucl. Sci. Eng. **153**, 93 (2006)
[19] R. Capote, et al., Nucl. Data Sheets **110**, 3107 (2009)
[20] W.P. Abfalterer, et al., Phys. Rev. C **63**, 044608 (2001)
[21] M. Ibaraki, et al., J. Nucl. Sci. Tech. S**2**, 405 (2002)
[22] A. Negret, et al., Phys. Rev. C **88**, 027601 (2013)
[23] D. Schmidt, et al., PTB-N-20 (1994)
[24] J.K. Dickens, et al., ORNL-TM-11671 (1990)
[25] Xichao Ruan, et al., China Sci. Tech.**43**, 793 (2009)
[26] S. Matsuyama, et al., JAERI-M-92-027, 309 (1992)
[27] D. Soda, et al., JAERI-C-96-008, 146 (1995)
[28] H. Arakawa, et al., JAEA-C-2008-006, 58 (2008)
[29] I. Slypen, et al., J. Phys. G **30**, 45 (2004)
[30] V. Blideanu, et al., Phys. Rev. C **70**, 014607 (2004)
[31] R. Bevilacqua, et al., Nucl. Instr. Meth. A **646**, 100 (2011)
[32] C. Zanelli, et al., Phys. Rev. **C 23**,1015 (1981)